Roles of Equatorial Waves and Western Boundary Reflection in the Seasonal Circulation of the Equatorial Indian Ocean

DONGLIANG YUAN

Institute of Oceanology, Chinese Academy of Sciences, and First Institute of Oceanography, State Oceanic Administration, Qingdao, China

WEIQING HAN

PAOS, University of Colorado, Boulder, Colorado

(Manuscript received 17 May 2005, in final form 26 October 2005)

ABSTRACT

An ocean general circulation model (OGCM) is used to study the roles of equatorial waves and western boundary reflection in the seasonal circulation of the equatorial Indian Ocean. The western boundary reflection is defined as the total Kelvin waves leaving the western boundary, which include the reflection of the equatorial Rossby waves as well as the effects of alongshore winds, off-equatorial Rossby waves, and nonlinear processes near the western boundary. The evaluation of the reflection is based on a wave decomposition of the OGCM results and experiments with linear models. It is found that the alongshore winds along the east coast of Africa and the Rossby waves in the off-equatorial areas contribute significantly to the annual harmonics of the equatorial Kelvin waves at the western boundary. The semiannual harmonics of the Kelvin waves, on the other hand, originate primarily from a linear reflection of the equatorial Rossby waves. The dynamics of a dominant annual oscillation of sea level coexisting with the dominant semiannual oscillations of surface zonal currents in the central equatorial Indian Ocean are investigated. These sea level and zonal current patterns are found to be closely related to the linear reflections of the semiannual harmonics at the meridional boundaries. Because of the reflections, the second baroclinic mode resonates with the semiannual wind forcing; that is, the semiannual zonal currents carried by the reflected waves enhance the wind-forced currents at the central basin. Because of the different behavior of the zonal current and sea level during the reflections, the semiannual sea levels of the directly forced and reflected waves cancel each other significantly at the central basin. In the meantime, the annual harmonic of the sea level remains large, producing a dominant annual oscillation of sea level in the central equatorial Indian Ocean. The linear reflection causes the semiannual harmonics of the incoming and reflected sea levels to enhance each other at the meridional boundaries. In addition, the weak annual harmonics of sea level in the western basin, resulting from a combined effect of the western boundary reflection and the equatorial zonal wind forcing, facilitate the dominance by the semiannual harmonics near the western boundary despite the strong local wind forcing at the annual period. The Rossby waves are found to have a much larger contribution to the observed equatorial semiannual oscillations of surface zonal currents than the Kelvin waves. The westward progressive reversal of seasonal surface zonal currents along the equator in the observations is primarily due to the Rossby wave propagation.

1. Introduction

Indian Ocean circulation is subject to large seasonal variations because of the strong forcing by the Indian Ocean monsoon. The effects of surface winds on the upper-ocean circulation of the Indian Ocean have been studied by Luther and O'Brien (1985), Woodbury et al. (1989), and McCreary et al. (1993). Over the equatorial region, existing studies on the seasonal circulation have focused on zonal currents, especially the semiannual eastward-flowing surface jets during spring and autumn, which are commonly referred to as the Wyrtki jets (Wyrtki 1973; O'Brien and Hurlburt 1974; Knox

Corresponding author address: Dongliang Yuan, Laboratory of Ocean Circulation and Waves, IOCAS, 7 Nanhai Road, Qingdao 266071, China.
E-mail: d_yuan2000@yahoo.com

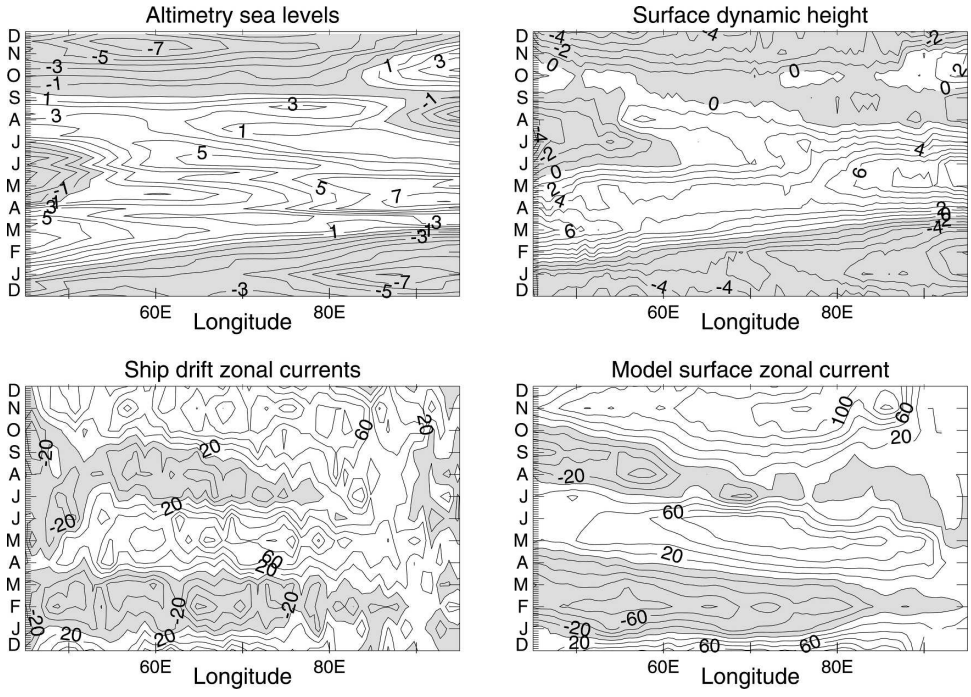

FIG. 1. Comparisons of the OGCM-simulated seasonal evolution of surface dynamic height (cm) and zonal current (cm s^{-1}) with TOPEX/Poseidon altimetry and ship drift data along the equator (1°S–1°N average). The altimetry data are based on the climatological data of 1993–2000.

1976; Luyten and Roemmich 1982; McPhaden 1982a,b; Gent et al. 1983; Reverdin 1987; Jensen 1993; Han et al. 1999; Reppin et al. 1999). Results from these studies suggest that these Wyrtki jets are primarily forced by the semiannual winds over the equatorial area and a resonant excitation of the second baroclinic mode has been suggested (Jensen 1993; Han et al. 1999).

For the resonant response to wind forcing, the reflections of equatorial waves at the meridional boundaries are important. The study of Han et al. (1999) has demonstrated that the reflected Rossby waves from the eastern boundary play an important role in the strength and structure of the Wyrtki jets. The role of the western boundary reflection, however, has never been demonstrated explicitly. Traditional understanding of the western boundary reflection is in the linear theory of Cane and Sarachik (1977) and Cane and Gent (1984), which calculates the Kelvin wave amplitude from the incoming equatorial Rossby waves based on a balance of the mass fluxes carried by these waves. However, recent analyses of the altimetry data show significant discrepancies from this theory both in the western Indian Ocean (Le Blanc and Boulanger 2001) and in the western Pacific Ocean (Boulanger and Fu 1996; Zang et al. 2002). The wave reflectivity obtained by Yuan et al. (2004) and Yuan (2005) from an ocean general circulation model (OGCM) of the equatorial Pacific Ocean is also significantly different from this theory. The study of Spall and Pedlosky (2005) even suggests that the reflection is nonlinear. In the western Indian Ocean, strong alongshore winds vary seasonally off the east coast of Africa, which can force coastal Kelvin waves propagating to the equator. There is also an indication that the off-equatorial Rossby waves force significant current variations along the western boundary (McCreary et al. 1993). The importance of the alongshore winds and off-equatorial Rossby waves to the equatorial circulation has not been examined explicitly so far.

Ocean Topography Experiment (TOPEX)/Poseidon altimeter data have shown a dominant annual oscillation of sea level in the central equatorial Indian Ocean (Fig. 1). This annual oscillation is over an equatorial domain where strong semiannual oscillations of surface zonal currents dominate. In the western and eastern basins, however, the seasonal sea level is dominated by semiannual oscillations. These sea level patterns are consistent with the analysis of Reverdin (1987), which shows that the seasonal variation of thermocline depth in the central equatorial Indian Ocean from 55° to 80°E is dominated by an annual oscillation whereas those in the western and eastern basins are dominated by semiannual oscillations. How the equatorial waves produce the distinctly different characters of the seasonal sea level (thermocline) and surface zonal currents has not

been explained before. The sea level and thermocline variations over the equatorial Indian Ocean are important because they are related to the equatorial upwelling, which is important to upper-ocean thermodynamics and biogeochemical processes.

The objectives of this paper are to understand the effects of equatorial winds, alongshore winds near the western boundary, off-equatorial Rossby waves, and the western boundary reflection of the equatorial Rossby waves on the seasonal circulation of the equatorial Indian Ocean. The rest of the paper is organized as follows. Section 2 describes the configuration of the models. In section 3, the OGCM simulation is decomposed into equatorial Kelvin and Rossby waves, based on which the western boundary reflection and its effects on the equatorial seasonal sea level and surface zonal currents are studied. Section 4 contains a discussion and summary.

2. Ocean models

A hierarchy of ocean models is used in this study: an OGCM, a linear continuously stratified model (LCSM), and a linear equatorial wave model based on the integration, along the wave characteristic lines, of the zonal wind stress projected onto the equatorial wave modes.

a. The OGCM

The OGCM is the Hybrid Coordinate Ocean Model (HYCOM), which is used to produce a realistic simulation of the seasonal circulation in the tropical Indian Ocean. The HYCOM is configured over the Indian Ocean north of 30°S with a horizontal resolution of $0.5° \times 0.5°$ (Han et al. 2004; Han 2005). Realistic basin geometry and topography are used, and 18 layers with a fine resolution in the upper ocean are chosen to better resolve the vertical structures of upper-ocean currents, the mixed layer, and the thermocline. The nonlocal *K*-profile parameterization (KPP) is adopted for the surface mixed layer scheme (Large et al. 1994, 1997).

Along the continental boundaries, no-slip boundary conditions are applied. Near the southern boundary, a sponge layer of 5° (25°–30°S) is used to relax the model temperature and salinity to Levitus and Boyer (1994) and Levitus et al. (1994) climatologies, respectively. Lateral boundary forcing due to the Indonesian Throughflow is included by relaxing the model temperature and salinity to the Levitus data in the throughflow region.

The surface wind stress used to force the model is derived from the Florida State University (FSU) monthly pseudo–wind stress climatology. Surface heat and freshwater fluxes are derived from the wind speed, air temperature, specific humidity, surface net shortand longwave radiation, and precipitation of the Comprehensive Ocean Atmosphere Data Set (COADS). Penetrative heat flux of shortwave radiation is considered using the Jerlov water type IA (Jerlov 1976). The model is spun up from a state of rest for 21 yr. The structures of the dynamic height and zonal currents on the equator in year 21 are similar to a 5-yr average of year 21–25. The results shown in this paper are from year 21.

b. The LCSM

The LCSM is used to estimate the relative importance of equatorial zonal winds, alongshore winds along the western boundary, and the winds in the off-equatorial areas for the equatorial ocean circulation. A comparison with the OGCM solution also helps to identify nonlinear effects. The LCSM used here is similar to that reported by McCreary (1981), except that the annual mean density profile averaged over the 5°S–5°N equatorial region from the OGCM is used to calculate the baroclinic mode speeds and the wind coupling coefficients. The model basin and horizontal resolution are the same as those of the OGCM. The coefficients of horizontal Laplacian mixing and Newtonian cooling are specified as 10^4 m^2 s^{-1} and 10^{-9} s^{-1}.

c. The linear wave model

A simple linear wave model is used to understand the effects of western boundary reflection on the equatorial circulation. The solution of this model is obtained by projecting the zonal wind stress onto the equatorial Kelvin and Rossby modes and by integrating the projected coefficients along the characteristic lines of the equatorial waves. As in the LCSM, the wave speeds and wind coupling coefficients of the baroclinc modes are calculated using the averaged mean density profile from the OGCM over the equatorial basin. The Kelvin wave equation is integrated eastward from the decomposed (or reflected) Kelvin wave coefficients at 49°E. The Rossby wave equation is integrated westward from 95°E. Linear friction is added with a coefficient of 10^{-11} s^{-1}, which is based on the background viscosity and the maximum buoyancy frequency. The solutions are not sensitive to the friction coefficient at such a small value.

3. Results

In this section, we first compare the OGCM solution with observations to validate the model results (section

3a). Then we analyze the OGCM results and linear model solutions to assess the effects of the equatorial waves, western boundary reflection of the equatorial Rossby waves, alongshore winds along the western boundary, and the off-equatorial Rossby waves on the equatorial circulation, respectively, in section 3b. Dynamics of the annual and semiannual harmonics as well as effects of nonlinearity are discussed in section 3c. Last, the seasonal cycles of sea level and surface zonal current are reconstructed from the decomposed waves in section 3d to quantify the roles of the equatorial waves explicitly.

Throughout this paper, the seasonal variations are defined as the de-meaned monthly averages.

a. The simulated seasonal cycle

Figure 1 shows the observed and OGCM-simulated seasonal variations of sea level and surface zonal current along the Indian Ocean equator. The model surface dynamic height has been adjusted with the seasonal atmospheric surface pressure of the National Centers for Environmental Prediction (NCEP). The adjustment turns out to be small. The simulated sea level and surface zonal current agree reasonably with the observations. The dominant semiannual variations of sea level in the western and eastern basins and the dominant annual variation in the central basin shown in the TOPEX/Poseidon data are simulated well by the OGCM. The dominant semiannual oscillations of the surface zonal current over the equatorial Indian Ocean are also in good agreement with the ship drift data. The model pycnocline is slightly diffuse as compared with the Levitus climatological data (not shown). In particular, the maximum buoyancy frequency at the subsurface in the observations has been underestimated in the model. However, comparisons of the vertical modes using the simulated mean stratification with those using the Levitus data show good agreement for the low-order modes in terms of depths of the zero crossings and the magnitudes near the sea surface (figure omitted). This suggests that the simulated waves bear the significance of the seasonal cycle waves in nature.

The annual and semiannual harmonics of the observed and simulated sea level and surface zonal currents in Fig. 1 are compared in Fig. 2. Overall, the model has done a good job of reproducing the observed annual and semiannual harmonics in the sea level and surface zonal current fields. In particular, the minimum semiannual harmonic of sea level and the maximum semiannual harmonic of zonal current in the central equatorial Indian Ocean are reproduced well both in amplitudes and in phases.

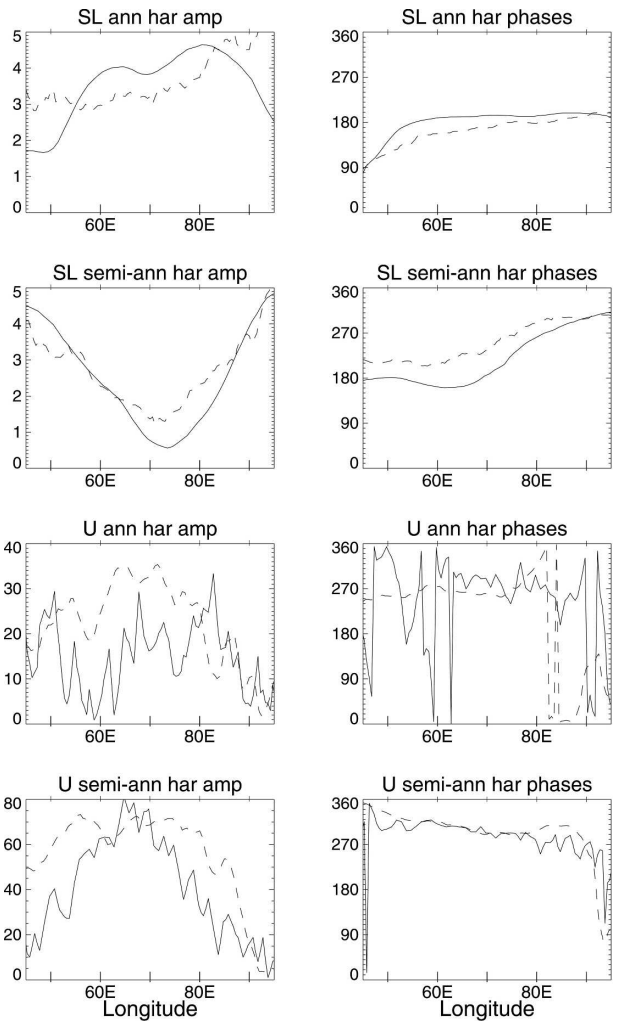

FIG. 2. Comparison of the annual and semiannual harmonics of the simulated sea level (SL) and zonal current (U) with those of the altimetry and ship drift data. Units are centimeters for sea level amplitudes, centimeters per second for current amplitudes, and degrees for the phases. Solid curves are for the observations, and dashed curves are for model results.

b. The wave dynamics in the OGCM and LCSM

The OGCM solution is decomposed into equatorial waves to study the seasonal cycle dynamics. The eigenfunctions and wave speeds of the baroclinic modes were first calculated based on the averaged density profile over 5°S–5°N. The three-dimensional dynamic height and zonal velocity in reference to 2500-m depth were then projected onto the eigenfunctions to extract the coefficients associated with each baroclinic mode, which were further decomposed into equatorial Kelvin and Rossby waves according to the procedure described by Yuan et al. (2004). The procedure is essentially the same as in Minobe and Takeuchi (1995) and Boulanger and Menkes (1995), except that the OGCM

zonal currents instead of the geostrophic zonal currents were used in the decomposition. The use of the model zonal currents ensures the complete nonlinear zonal momentum balance of the OGCM in the decomposed waves (Yuan et al. 2004). The horizontal structures of the decomposed wave coefficients are not sensitive to the density profile used in the calculation (Boulanger and Menkes 1995). Uses of the density profiles of the western and eastern equatorial Indian Ocean yield essentially the same decomposed wave coefficient structures.

1) THE FIRST BAROCLINIC MODE

Figure 3 shows the Kelvin and the first through third meridional-mode Rossby wave coefficients of the first baroclinic mode decomposed from the OGCM solution. The positive (negative) contours indicate downwelling (upwelling) waves all through this paper. The Kelvin waves exhibit a semiannual dominant oscillation originating from the western boundary and propagate eastward. The speeds of the propagation are not exactly the same as the first eigenvalue of the vertical mode separation (indicated by the straight line in the top-left panel in Fig. 3) because of wind forcing and oceanic nonlinearity. The upwelling Kelvin waves originating from the western boundary in winter and summer can be identified from the altimetry data in Fig. 1 and appear to be strengthened by the equatorial easterlies, especially in winter (Fig. 4). The connection between the low sea level near the western and eastern boundaries in summer in the altimetry data is indicated by the Kelvin wave coefficients. The first meridional-mode Rossby waves of the first baroclinic mode originating from the eastern boundary also exhibit a dominant semiannual oscillation and are qualitatively in phase with the arrival of the Kelvin waves at the eastern boundary. The first meridional-mode Rossby waves propagate westward at a speed of roughly 1/3 of the Kelvin wave speed, in agreement with the linear wave theory. The downwelling and upwelling first meridional-mode Rossby waves during summer through winter are enhanced by the equatorial winds (Fig. 4). The downwelling first meridional-mode Rossby waves generated in the central basin since December and arriving at the western basin in late January are generated by winds instead of eastern boundary reflection, because they are detached from the eastern boundary. The upwelling Rossby waves from the eastern boundary during December–March, however, are dominated by eastern boundary reflection and are weakened substantially by the winds.

The second meridional-mode Rossby waves of the first baroclinic mode are generated primarily by winds in the central-eastern equatorial Indian Ocean as evidenced by the agreement with the wind projection and by the discontinuity of the waves with those from the eastern boundary. These waves participate in the western boundary reflection in the linear theory because of the inclined western boundary geometry. The third meridional-mode Rossby waves exhibit an annual dominant character in the central and eastern basins and a semiannual dominant oscillation in the west.

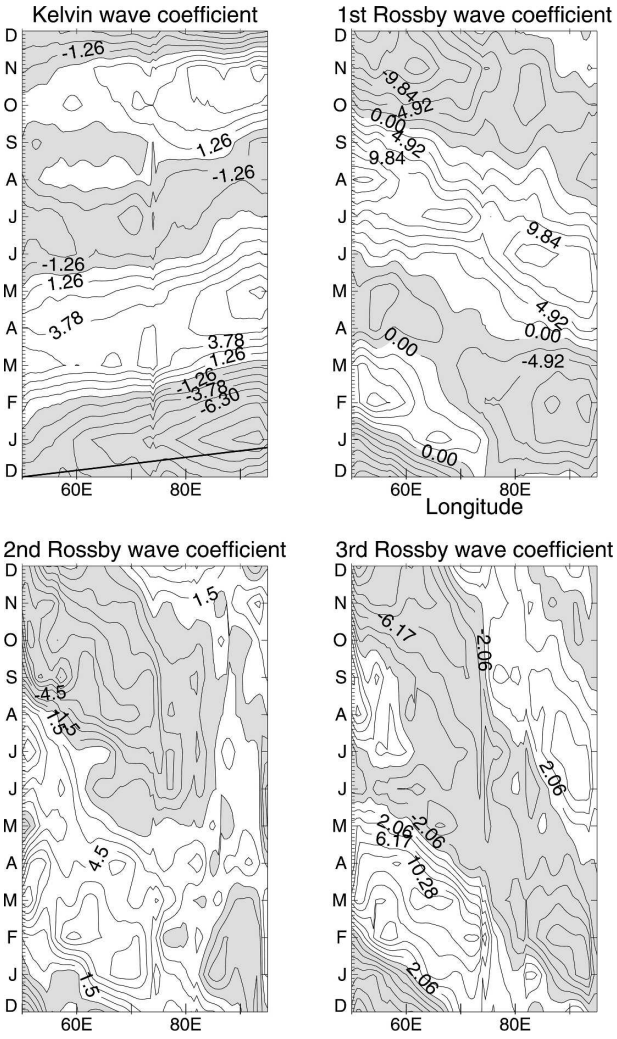

FIG. 3. Coefficients of decomposed Kelvin and the first three meridional-mode Rossby waves of the first baroclinic mode. The contour units correspond to 0.33 m and 1.31 cm s^{-1} for Kelvin wave sea level and surface zonal current on the equator, 0.14 m and -1.61 cm s^{-1} for the first meridional-mode Rossby waves, and 0.04 m and 1.23 cm s^{-1} for the third meridional-mode Rossby waves. Note that sea level and surface zonal current have the same sign for the Kelvin wave but opposite signs for the first meridional-mode Rossby wave on the equator. The sea level and surface zonal current represented by the second meridional-mode Rossby waves are zero on the equator. The thick straight line at the bottom of the Kelvin wave panel marks the linear free Kelvin wave speed.

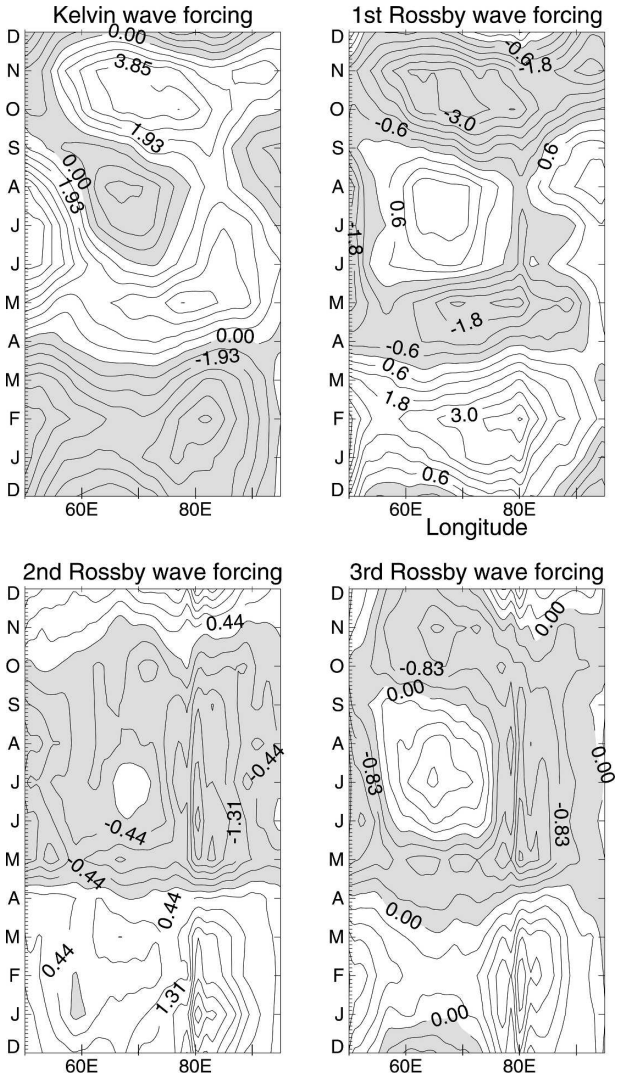

FIG. 4. Wind stress projected onto the Kelvin and first three meridional-mode Rossby waves of the first baroclinic mode (N m^{-2}).

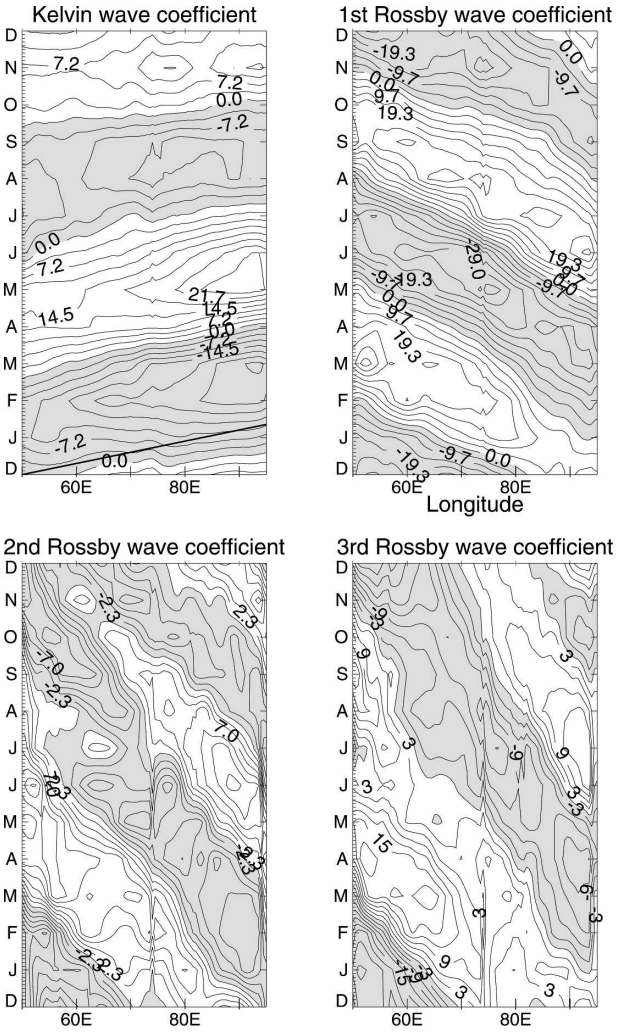

FIG. 5. Same as in Fig. 3 but for the second baroclinic mode. The dimensional amplitudes for sea level and surface zonal current on the equator represented by unit wave coefficients are those of the first baroclinic mode waves multiplied by $c_2/c_1 = 0.58$ for surface zonal current and $c_2^2/c_1^2 = 0.34$ for sea level.

The projected zonal wind stress on the Kelvin and first meridional-mode Rossby waves of the first baroclinic mode in Fig. 4 shows that the zonal wind forcing on these waves over the equatorial Indian Ocean is dominated by annual oscillations in the eastern and western basins and by semiannual oscillations in the central basin. The annual and semiannual harmonics of the total wind stress calculated by Han et al. (1999) show that the maximum annual harmonic exists near the western boundary and a secondary maximum is located at around 80°E. The semiannual harmonics are the largest and dominate the annual harmonics over the domain of 60°–80°E. Near the western boundary and east of 80°E, the annual harmonics dominate. The locations of the maximum annual and semiannual wind forcing play an important role in the annual and semiannual dominant patterns of the equatorial Indian Ocean sea level (see later).

2) THE SECOND BAROCLINIC MODE

The Kelvin and the first meridional-mode Rossby waves of the second baroclinic mode also exhibit semiannual dominant oscillations originating from the western and eastern boundaries, respectively (Fig. 5). The second and third meridional-mode Rossby waves of the second baroclinic mode, on the other hand, exhibit semiannual dominant oscillations in the eastern basin but annual dominant oscillations near the western boundary (lower panels in Fig. 5). The structures of the

wind stress projected onto the second baroclinic mode waves are similar to, except for a larger amplitude than, those on the first baroclinic waves, and their figures are not shown here. The magnitudes of the second baroclinic waves are much larger than those of the first baroclinic waves, because of the larger wind stress projected onto the second baroclinic mode and the near-resonant forcing of the second baroclinic mode (Gent et al. 1983; Reverdin 1987; Han et al. 1999).

In Fig. 5, it is clear that the sea level variations of the Kelvin and the first meridional-mode Rossby waves are out of phase in the central basin and cancel each other significantly. The zonal currents of the two kinds of waves, on the other hand, enhance each other in the central basin, because the positive (negative) Rossby wave coefficients correspond to westward (eastward) zonal current variations on the equator. The constructive interference of the zonal current of the second baroclinic waves gives rise to a resonant response of the zonal currents to the semiannual dominant wind forcing in the central basin, the dynamics of which have been studied by existing studies (Jensen 1993; Han et al. 1999). The destructive interference of the sea level, which has not been studied so far, results in the minimum semiannual harmonic in the central basin (Fig. 2). We will return to this point later in this paper.

3) Reflection at the western boundary

The time series of the decomposed equatorial Kelvin wave near the western boundary (49°E) are compared with that of the synthetic equatorial Kelvin wave in Fig. 6. The synthetic Kelvin wave is the sum of the Kelvin waves reflected from each Rossby wave at an infinite meridional wall at 43°E, based on the linear reflection theory of Cane and Sarachik (1977). The Kelvin wave amplitudes reflected from the first and the third meridional-mode Rossby waves are 0.41 and 0.13 of their corresponding Rossby wave amplitudes, respectively (Boulanger and Menkes 1995). The contribution from the antisymmetric, even-mode Rossby waves is zero in this case. The contribution from the Rossby waves higher than the third meridional mode is small and is truncated here. The phase lag for the contribution of each Rossby wave is calculated based on the distance from the western boundary. In Fig. 6, the synthetic Kelvin waves with and without the zonal wind forcing west of 49°E are shown by diamond and cross curves, respectively. The effects of zonal wind west of 49°E are calculated by integrating the Rossby wave equation westward, starting from the decomposed Rossby wave coefficients at 49°E, and the Kelvin wave equation eastward, starting from zero condition at the African coast, forced with the zonal wind stress projected onto these

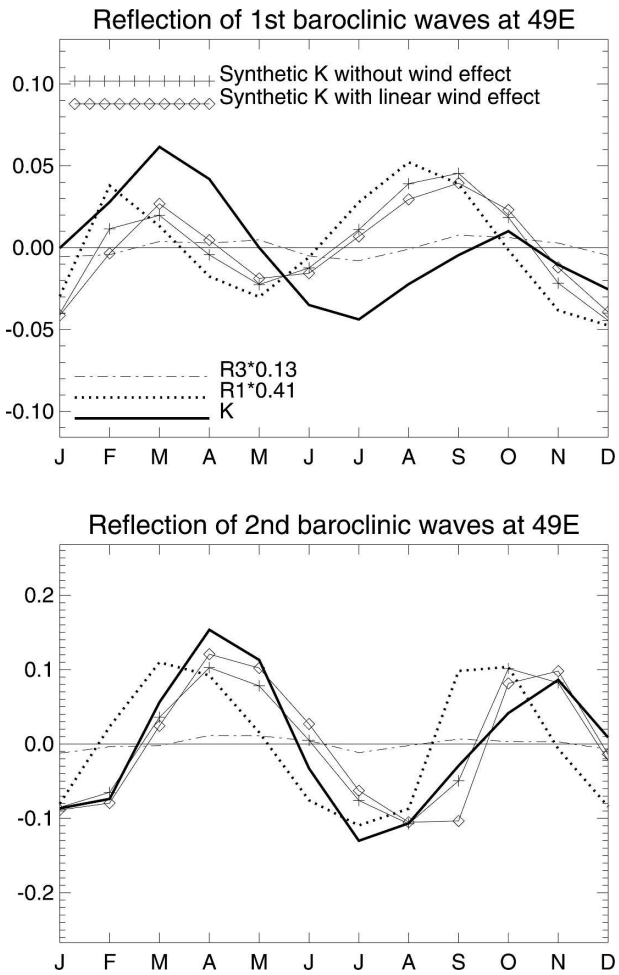

FIG. 6. Coefficients of the Kelvin and first three meridional-mode Rossby waves of the (top) first and (bottom) second baroclinic modes at the western boundary. The Rossby wave coefficients have been multiplied by their Kelvin wave reflection ratios. Synthetic Kelvin waves of linear reflection at an infinite meridional western boundary are drawn with diamond and cross curves for comparisons. The diamond curve has the zonal wind effects west of 49°E included. The cross curve assumes no wind forcing west of 49°E.

waves. The Rossby waves are assumed to be reflected at 43°E and are superposed, with proper time lags, onto the integrated equatorial Kelvin wave to obtain the Kelvin wave amplitudes at 49°E. The small difference between the diamond and the cross curves suggests that the effects of the equatorial zonal wind stress west of 49°E are small.

The top panel in Fig. 6 indicates that the decomposed first baroclinic mode Kelvin wave is significantly different from a linear reflection of equatorial Rossby waves at the western boundary. The decomposed Kelvin wave coefficients are much larger than the synthetic Kelvin wave coefficients during winter–spring and smaller dur-

ing summer–autumn. This difference may result from various causes: forcing due to alongshore winds near the western boundary, off-equatorial Rossby waves generated by off-equatorial winds, and nonlinearity of the oceanic system. These effects will be examined in section 3b(4). The inclined western boundary, which makes the reflection frequency dependent, has a small effect on the synthetic reflection at annual and semiannual periods. When an angle of 45° with the equator is considered for the western boundary, the reflected amplitude ratios of the Kelvin wave from the first through the third meridional-mode Rossby waves are 0.41, 0.06*i*, and 0.12, respectively, for the annual harmonics and 0.40, 0.11*i*, and 0.08, respectively, for the semiannual harmonics according to the Cane and Gent (1984) theory. The imaginary coefficients for the second meridional-mode Rossby waves indicate a phase lead of 90° during the reflection. The small ratios of the second meridional-mode Rossby waves suggest that the inclination of the western boundary has a small effect on the reflection of low-frequency waves, especially for the annual harmonics.

Comparisons of annual and semiannual harmonics suggest that the difference between the decomposed and synthetic Kelvin waves is primarily in the annual harmonic (Fig. 7). *The annual harmonics of the decomposed and synthetic Kelvin waves of the first baroclinic mode are in opposite phases to each other* (top panel in Fig. 7). In contrast to the annual harmonics, the decomposed and synthetic semiannual harmonics agree with each other very well except for a small phase difference (bottom panel in Fig. 7). The small phase difference could be due to the uncertainty of the reflection longitude. If the reflection were assumed at 40°E, the two semiannual harmonics would agree with each other very well. These results are consistent with the fact that the semiannual wind forcing is concentrated over the equatorial area (Hastenrath and Greischar 1991).

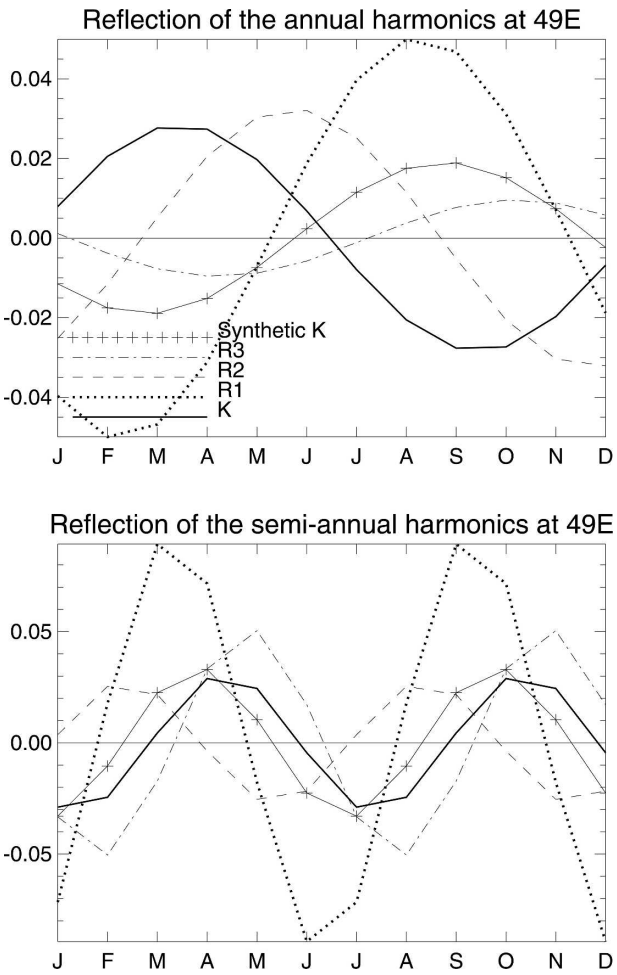

FIG. 7. (top) Annual harmonics and (bottom) semiannual harmonics of the Kelvin and the first three meridional-mode Rossby waves of the first baroclinic mode at the western boundary. Synthetic Kelvin waves according to the linear reflection theory are drawn with the cross curves for comparison.

In contrast to the reflection of the first baroclinic mode, the decomposed and synthetic Kelvin waves of the second baroclinic mode agree with each other well at the western boundary (bottom panel in Fig. 6). The better agreement is because the second baroclinic mode is dominated by semiannual harmonics, which are in resonance with the equatorial semiannual wind forcing (Jensen 1993; Han et al. 1999).

4) EFFECTS OF ALONGSHORE, OFF-EQUATORIAL, AND EQUATORIAL WINDS

Given that the difference between the decomposed and synthetic Kelvin waves exists primarily in the first baroclinic mode, the responses of the first baroclinic mode to various wind forcing are investigated to understand the relative importance of the alongshore, the off-equatorial, and the equatorial winds on the equatorial circulation. Three experiments are conducted using the LCSM for this purpose: the main run (MR), which is forced by the FSU winds over the entire model domain; test run 1 (TR1), which is forced by modified FSU winds with the winds west of 60°E set to zero; and test run 2 (TR2), which is forced only by the equatorial winds between 5°S and 5°N and east of 60°E. For all of these experiments, the LCSM is integrated forward from a state of rest for 5 yr and the results of year 5 are decomposed into equatorial Kelvin and Rossby waves.

The top panel in Fig. 8 shows the decomposed Kelvin wave (thick solid curve) and the first and the third meridional-mode Rossby waves (dash and dot curves) of the first baroclinic mode at 49°E together with the syn-

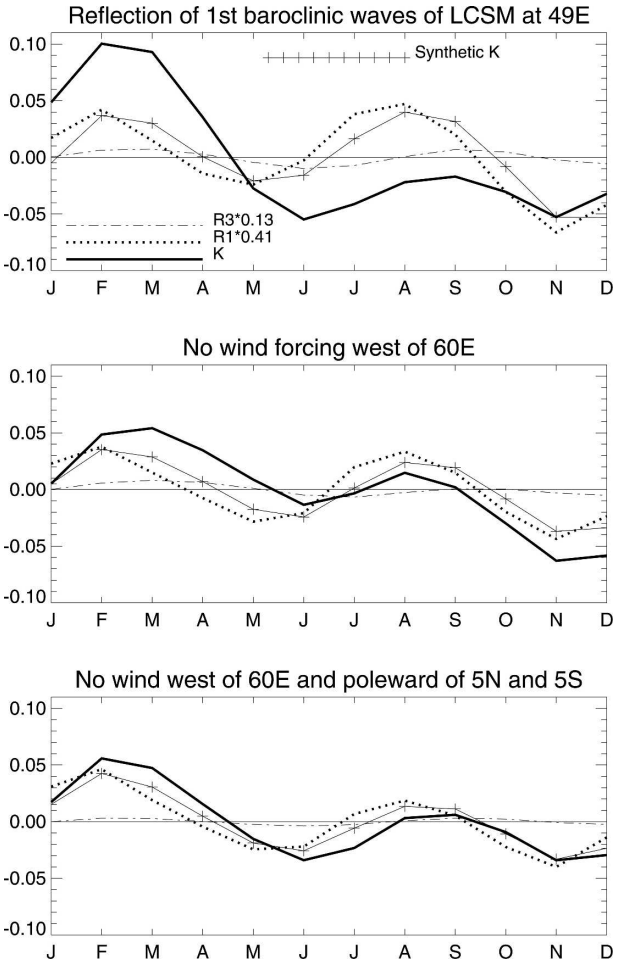

FIG. 8. Each panel is the same as the top panel in Fig. 6 except for the linear continuously stratified model experiments, which are forced with the (top) FSU winds, (middle) FSU winds east of 60°E, and (bottom) FSU winds east of 60°E and equatorward of 5°N and 5°S, respectively.

thetic Kelvin wave (cross curve) in the MR. These wave coefficients correspond to the OGCM solution shown in the top panel in Fig. 6. The Rossby waves and the synthetic Kelvin wave are similar to the OGCM results, suggesting that the essential dynamics of the OGCM are represented well by the simple model over the equatorial area.

Similar to the OGCM results, the decomposed and synthetic Kelvin waves in the MR have a large discrepancy, with the decomposed Kelvin wave larger during winter–spring and smaller during summer–autumn than the synthetic Kelvin wave near the western boundary. This result suggests that the alongshore winds and off-equatorial winds may have an effect on the equatorial circulation, because the synthetic Kelvin wave only represents the reflection of the equatorial Rossby waves forced by the equatorial winds. The amplitudes of the decomposed Kelvin waves in the linear model, however, are much larger than in the OGCM. Since the LCSM has neglected the nonlinear terms, the difference indicates the significant role of nonlinearity of the oceanic system. The LCSM has a flat-ocean thermocline over the entire basin. In OGCM, the ocean thermocline depth changes considerably in the vicinity of the western boundary and in the off-equatorial area. The first baroclinic modes of the LCSM and OGCM indeed have sizable differences in the subtropical area and near the western boundary (not shown). A detailed study of the LCSM and GCM differences involves controlled experiments with the OGCM, which are too expensive to run at present. In the future, a more focused study may be conducted to resolve the issue.

The middle panel in Fig. 8 shows the solution from experiment TR1, which has excluded the winds in the western basin where the annual cycle of alongshore winds associated with the seasonally reversing monsoon is strong. The decomposed and synthetic Kelvin waves agree much better in TR1 than in MR, suggesting the significant role of the alongshore winds near the western boundary. There are still significant differences in the Kelvin wave amplitudes remaining in TR1, which turn out to be induced by the off-equatorial wind forcing. If the LCSM is forced only by the equatorial winds (solution TR2), the decomposed and synthetic Kelvin waves will agree very well (bottom panel in Fig. 8). The results of these controlled experiments suggest that coastal Kelvin waves generated by the alongshore winds and the off-equatorial Rossby waves contribute significantly to the equatorial circulation.

Figure 9 shows the sea level variations from the OGCM simulation during March, June, September, and December. The high sea level over the western equatorial area in March is evidently connected to the high sea level in the off-equatorial western basin and near the western boundary. This is the time when both the alongshore wind and off-equatorial Rossby waves produce downwelling Kelvin waves on the equator (Fig. 8). The low sea level in the western equatorial region during December is primarily produced by the reflection of the upwelling equatorial Rossby waves (Fig. 8), although some contribution can be traced to the low sea level in the Arabian Sea (see McCreary et al. 1993). During summer and autumn, the low sea level in the western equatorial region is connected to the low sea level along the western boundary, suggesting the importance of alongshore winds in affecting the equatorial circulation.

To estimate the relative importance of the alongshore plus off-equatorial winds, western boundary reflection of the equatorial Rossby waves, and the equa-

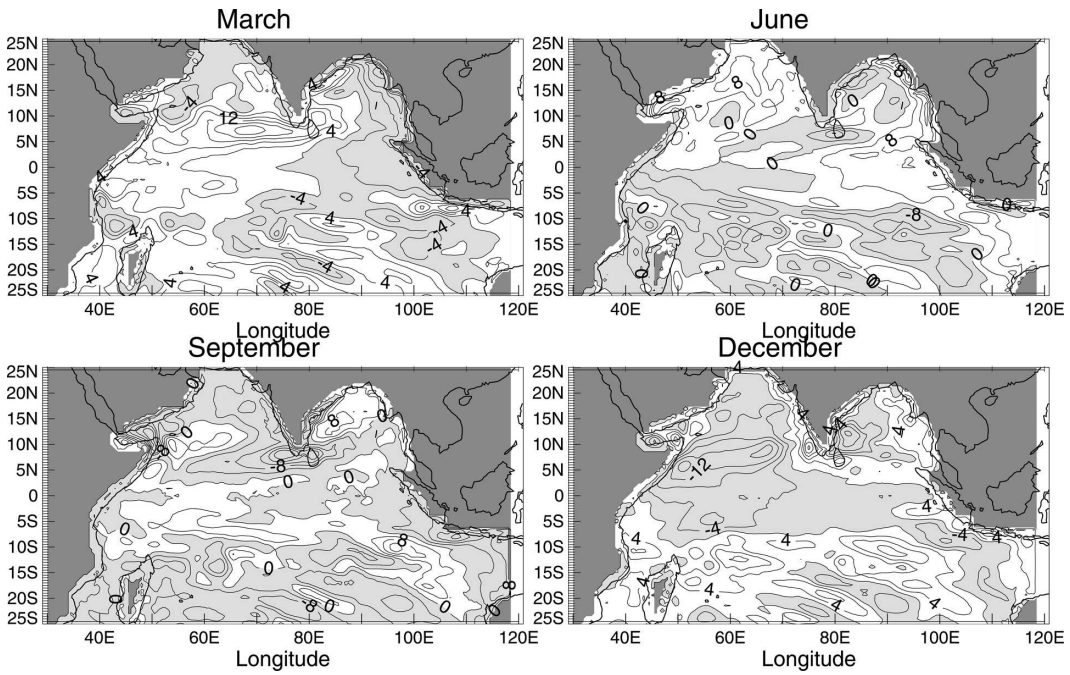

FIG. 9. Seasonal departures of surface dynamic height (cm) simulated by the OGCM.

torial winds in affecting the equatorial circulation in the OGCM solution, we plot out Fig. 10. To estimate the Kelvin waves caused by the combination of the alongshore winds, the off-equatorial winds, and western boundary reflection of the equatorial Rossby waves, the Kelvin wave equation is integrated eastward along the wave characteristic line, starting from the decomposed Kelvin wave coefficients at 49°E with no wind forcing (upper-left panel in Fig. 10). We refer to this solution as western boundary (WB) forced Kelvin waves. To isolate the western boundary reflection of the equatorial Rossby waves only, the Kelvin wave equation is integrated once more eastward starting from the synthetic Kelvin wave coefficients at 49° (lower-left panel in Fig. 10). This solution is referred to as equatorially reflected Kelvin waves. The difference between the two panels measures the effects of the alongshore and off-equatorial winds and oceanic nonlinearity near the western boundary. The total decomposed Kelvin waves are shown in the upper-right panel in Fig. 10, which are understood to be forced by the alongshore, off-equatorial, and equatorial winds, and affected by the nonlinearity of the oceanic system over the equatorial area (Yuan et al. 2004). The effects of equatorial winds and nonlinearity can be estimated by subtracting the WB-forced Kelvin waves (upper-left panel in Fig. 10) from the total decomposed Kelvin waves (upper-right panel). If the subtracted Kelvin waves are added onto the equatorially reflected Kelvin waves (lower-left panel in Fig. 10), we produce the Kelvin waves that are the same as the total Kelvin waves except without the effects of the alongshore and off-equatorial wind forcing and oceanic nonlinearity near the western boundary (lower-right panel). These Kelvin waves are referred to as equatorially forced Kelvin waves in the following text.

It is evident that the equatorially forced Kelvin waves show a much stronger annual oscillation than the total decomposed Kelvin waves (cf. lower-right and upper-right panels in Fig. 10). In particular, the upwelling Kelvin waves in summer are significantly weakened.

c. *The annual and semiannual harmonics*

The annual and semiannual harmonics of the decomposed and linear wind-driven Kelvin and first meridional-mode Rossby waves are calculated and those of the first and the second baroclinic modes are shown in Fig. 11. The nonlinear effect is estimated by comparing the harmonics of the decomposed waves with those of linear wind-driven waves. The harmonics of the equatorially forced Kelvin waves, which do not include the effects of the alongshore and off-equatorial wind forcing and oceanic nonlinearity near the western boundary in the OGCM, are also shown for comparisons (dotted curve). Evidently, the annual harmonic of the equatorially forced Kelvin wave of the first baroclinic mode is much stronger than and in opposite phase to that of the decomposed Kelvin wave (cf. the dotted and dashed

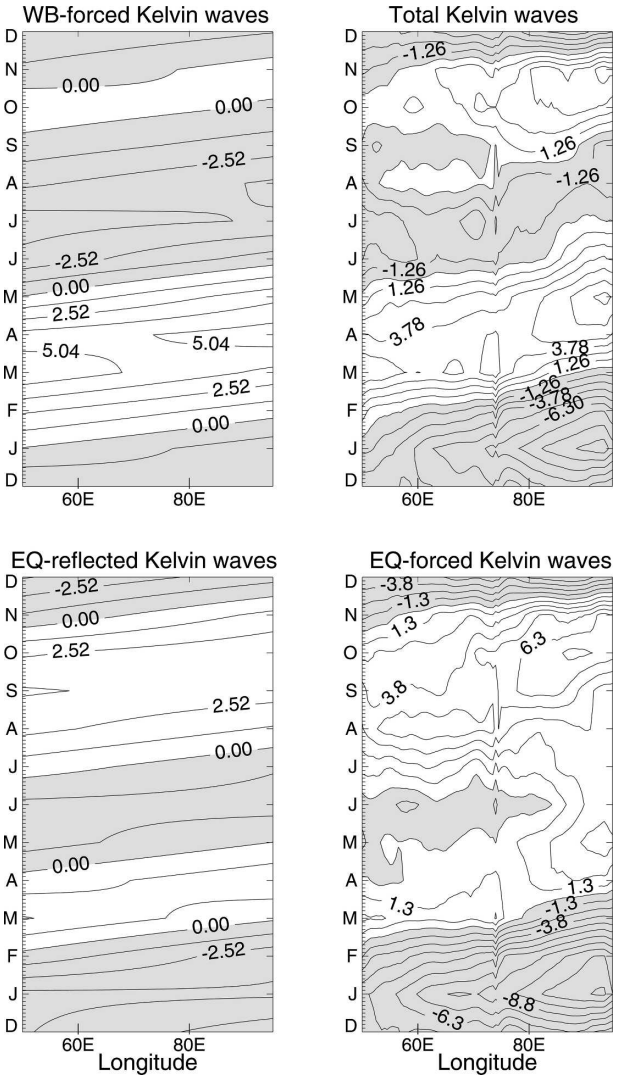

FIG. 10. Comparisons of the decomposed first baroclinic-mode Kelvin waves with those in a linear western boundary reflection scenario. The panels in the left column are Kelvin waves forced by the (top) nonlinear and (bottom) synthetic western boundary reflections. The panels in the right column are the total Kelvin waves; only the western boundary reflections are different. See text for the explanation of the Kelvin waves in the right column.

curves in the top two panels in Fig. 11a). The weak annual harmonic of the decomposed Kelvin wave in the western basin is produced because the zonal wind stress works against the Kelvin wave in the western basin, as indicated by the agreement between the decomposed and the linear wind-driven harmonics in the western basin (cf. the solid and dash curves). In comparison, the much stronger annual harmonic of the equatorially forced Kelvin wave is due to an in-phase forcing by the zonal winds in the western basin.

The weak annual harmonic of the decomposed Kelvin wave facilitates the dominance of the semiannual harmonic in the total sea level oscillation in the western basin. Here, the combined effects of the alongshore wind and the off-equatorial Rossby waves play an important role. If the decomposed Kelvin waves were to be replaced with the equatorially forced Kelvin waves, the sea level oscillation in the western basin would become annual dominant (see next section).

The annual harmonic of the first meridional-mode Rossby wave of the first baroclinic mode shows peak amplitudes in the western and central-eastern basins. The maxima of the annual harmonic are evidently associated with the zonal wind forcing as suggested by the agreement of the pattern with the linear wind-driven solution (solid curves). However, the linear wind-driven Rossby wave has underestimated the amplitudes of the decomposed annual harmonic significantly while reproducing the phase of the decomposed wave faithfully. Since the wave decomposition is essentially a first-integral estimate of the zonal nonlinear momentum equation, the amplitude difference suggests the importance of the nonlinear dynamics in modifying the wave amplitude. Large differences in amplitudes and agreement in phases between the decomposed and linear solutions are also found in the semiannual harmonics (second and fourth rows in Fig. 11a) and in the second baroclinic mode waves (Fig. 11b).

d. Reconstructed sea level and surface zonal current

Using the decomposed waves of the OGCM solution, the dynamics of the distinctive annual sea level and semiannual surface zonal current in the central equatorial Indian Ocean are now investigated. Figure 12 compares the simulated seasonal variations of the surface dynamic height and surface zonal current reconstructed from the decomposed Kelvin and the first meridional-mode Rossby waves of the first four baroclinic modes along the equator. The reconstructed fields (bottom panels in Fig. 12) basically reproduce the seasonal variations in the total OGCM solution (top panels) except for weaker amplitudes, which indicate that, while the Kelvin and first meridional-mode Rossby waves of the low-order baroclinic modes play a deterministic role in shaping the seasonal variations of sea level and surface zonal current, higher-order modes are important in modifying their amplitudes. The semiannual Wyrtki jets over the central equatorial Indian Ocean, the semiannual sea level fluctuations in the western and eastern basins, and the annual sea level oscillation in the central basin are all reproduced in the reconstructed fields. The dynamics of seasonal sea level and surface zonal current are evidently different. While the surface dynamic height is dominated by the Kelvin

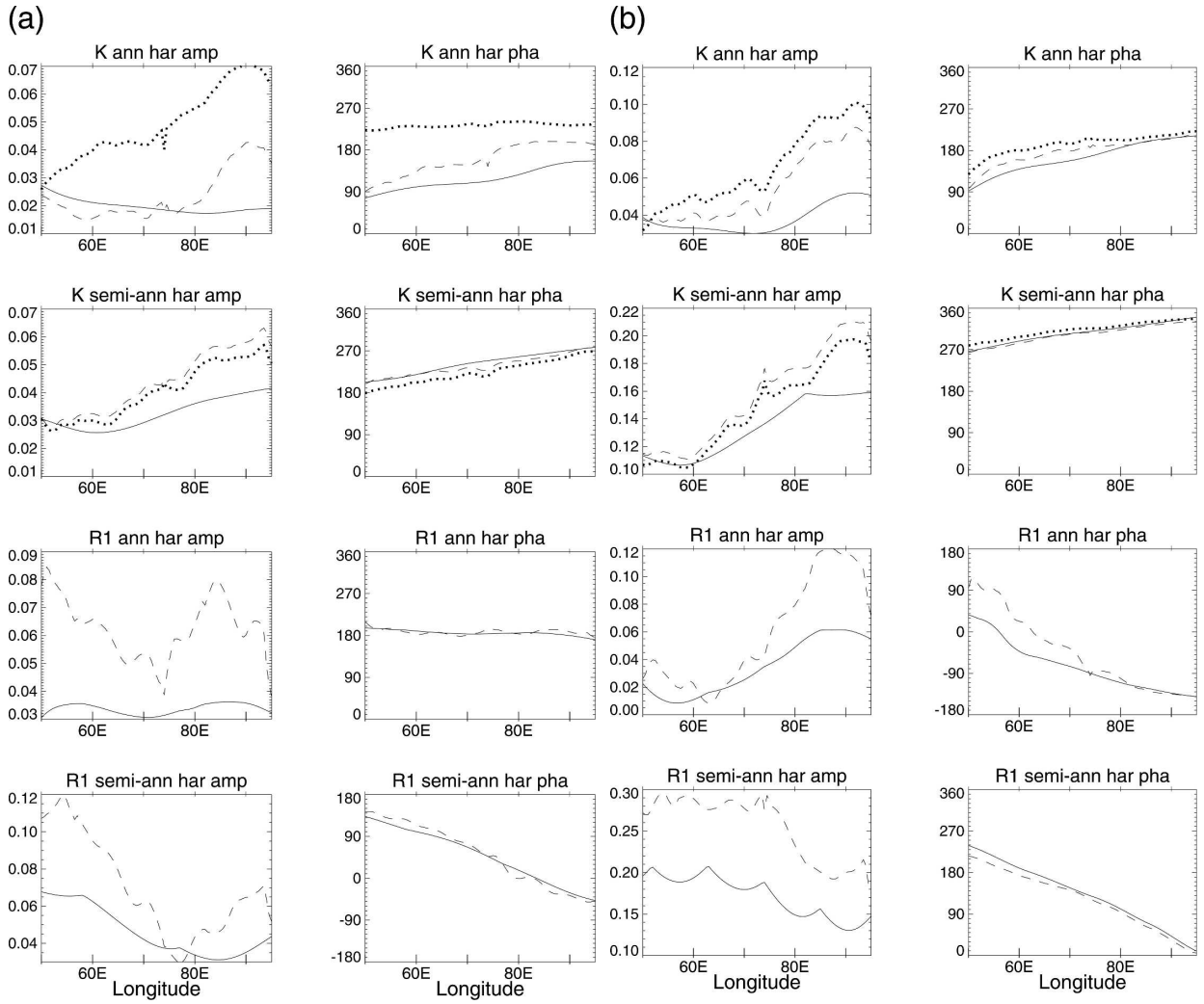

FIG. 11. (a) Comparison of amplitudes and phases of annual harmonics of the linear wind-forced (solid) and decomposed (dashed) Kelvin and the first meridional-mode Rossby waves of the first baroclinic mode. The annual harmonic of the Kelvin wave in a linear western boundary reflection scenario is also drawn with dotted curves in the upper panels for comparison. (b) Same as in (a) but for the second baroclinic-mode waves.

waves in the eastern basin and is contributed to significantly or even dominated by the Rossby waves in the western basin, the zonal surface current is primarily associated with the Rossby waves except over the eastern basin in winter, when the strong Kelvin waves generate large-amplitude westward flows (middle panels in the right column in Fig. 12). The different influence is due to the different structures of the Kelvin and Rossby waves. For the same sea level amplitude on the equator, the surface zonal current of the first meridional-mode Rossby wave is much larger than that of the Kelvin wave on the equator. The semiannual Rossby waves produce the eastward Wyrtki jets 2 times per year and the westward progressive reversal of the surface zonal currents, as observed in the ship drift data (Fig. 1).

From Fig. 12, it is clear that the semiannual sea level variations of the Kelvin and Rossby waves are out of phase and interfere destructively in the central equatorial basin. In contrast, the semiannual surface zonal currents associated with the Kelvin and Rossby waves are in phase and superpose constructively in the central basin. The constructive wave dynamics of the surface zonal currents have been discussed in earlier studies (Jensen 1993; Han et al. 1999), which are attributed to the resonant response of the second baroclinic mode with the semiannual wind forcing. The destructive wave dynamics of sea level in the central basin are also a result of the resonance as is evident in Fig. 12. The reason for the destructive interference of sea level at the central basin is because the sea level keeps its phase

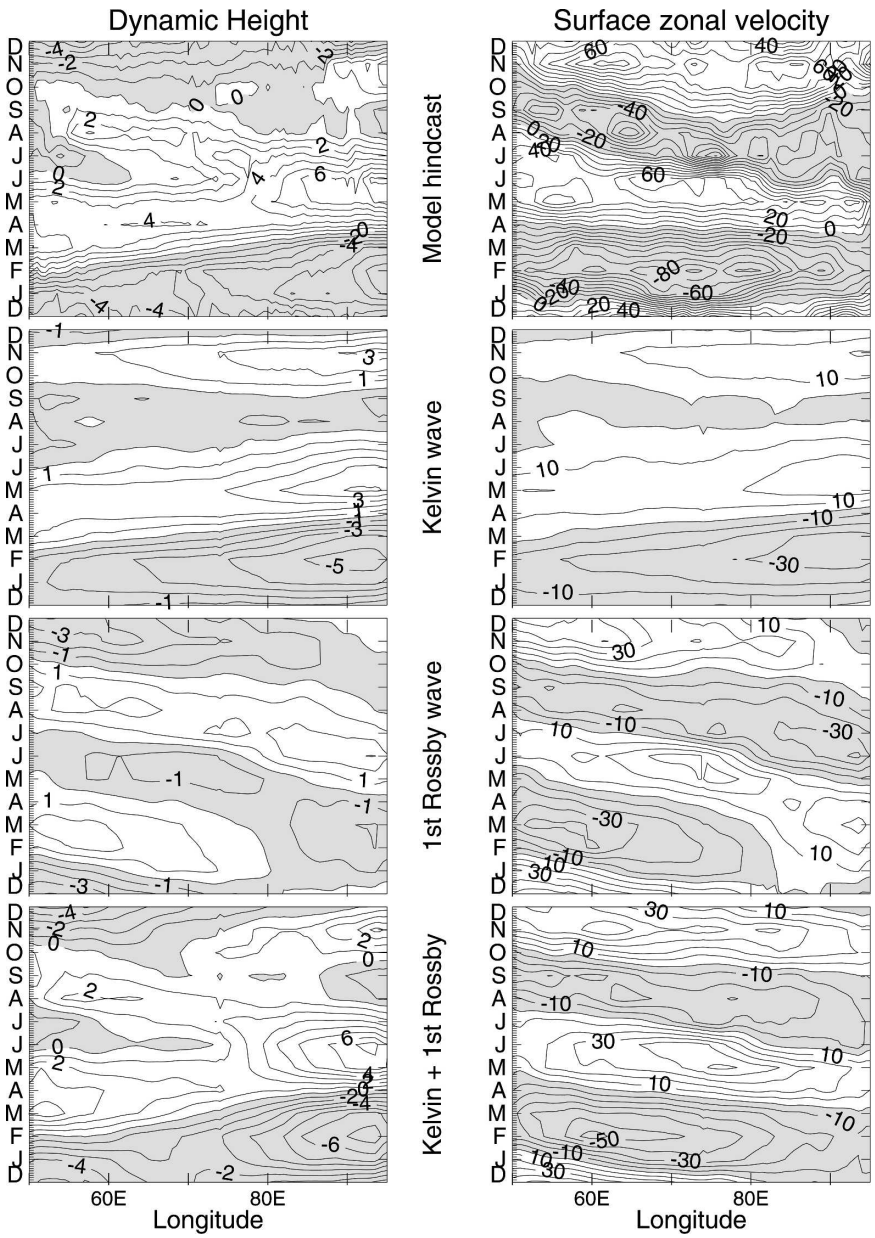

FIG. 12. Comparison of (top row) simulated and (rows 2–4) reconstructed seasonal variations of surface dynamic height (cm) and zonal current (cm s^{-1}) on the equator. The reconstructed variations are from the (second row) Kelvin waves and (third row) first meridonal-mode Rossby waves of the first four baroclinic modes. (bottom row) The summation of the second and third rows.

during the wave reflections at the meridional boundaries. In comparison, the zonal currents reverse phases during the reflections.

4. Discussion and summary

The Hybrid Coordinate Ocean Model and linear models are used to study the effects of equatorial waves and western boundary reflection on the seasonal circulation of the equatorial Indian Ocean. The western boundary reflection in this study is defined as the total equatorial Kelvin waves leaving the western boundary, which include the reflections of equatorial Rossby waves as well as the effects of alongshore winds, off-equatorial Rossby waves, and nonlinear processes of the OGCM near the western boundary. The evaluation

of the reflection is based on wave decomposition analyses of the OGCM and linear model results. The simulated seasonal cycles of sea level and surface zonal currents of the OGCM have been validated with the altimetry and ship drift data over the equatorial Indian Ocean.

The equatorial Kelvin waves originating from the western boundary are found to be significantly different from a linear reflection of the equatorial Rossby waves. The difference exists primarily in the annual harmonics. Experiments using a linear continuously stratified model suggest that the alongshore winds along the east coast of Africa and the off-equatorial Rossby waves can produce such a difference. The alongshore winds, which are dominated by the annually reversing monsoon, can force significant coastal Kelvin waves that propagate to the equator. The off-equatorial Rossby waves generated by the wind curl of the monsoon are also annual dominant and can force coastal Kelvin waves along the western boundary as well. Therefore, the annual harmonics of the equatorial Kelvin waves at the western boundary include not only the linear reflection of the equatorial Rossby waves, but also the contribution from the alongshore and off-equatorial wind forcing. The semiannual harmonics of the Kelvin waves, on the other hand, are in good agreement with the linear reflection of the equatorial Rossby waves, because the semiannual wind forcing is concentrated over the equatorial area.

The dominant annual oscillation of sea level coexisting with the dominant semiannual oscillation of surface zonal current in the central equatorial basin is a result of the linear reflections of the semiannual harmonics at the meridional boundaries. Because of the reflections, the zonal currents of the second baroclinic mode resonate with the semiannual wind forcing in the central basin; that is, the Rossby and Kelvin waves reflected from the meridional boundaries act to intensify the directly forced zonal currents (Han et al. 1999; section 3d). For example, in the central equatorial Indian Ocean where the semiannual winds have the maximum amplitude (Han et al. 1999), the westerly phase of the semiannual winds forces an eastward surface zonal current associated with downwelling Kelvin waves and upwelling Rossby waves. The Rossby waves are reflected into upwelling Kelvin waves at the western boundary. As the upwelling Kelvin waves arrive at the central basin, the semiannual winds reverse directions and drive upwelling Kelvin and downwelling Rossby waves. The westward zonal currents associated with the downwelling Rossby waves are intensified by the reflected upwelling Kelvin waves from the western boundary as shown in Fig. 12. However, the sea level variations of the reflected waves from the western boundary are in opposite phases with the directly forced sea level variations in the central basin. Thus, the wind-forced sea level variations in the central basin are weakened considerably by the reflected waves, resulting in a minimum semiannual harmonic of sea level there. The same processes also exist for the eastern boundary reflection. Nonlinearity of the system modifies this resonant response, but the essential dynamics remain.

In contrast, resonance does not occur at the annual period so that the annual harmonics of the Kelvin and Rossby wave sea level do not cancel in the central basin (Fig. 11). This explains the dominant annual oscillation of sea level in the central basin. In the western and eastern basins, the sea level variations are dominated by the semiannual cycle (Figs. 1 and 12), because the semiannual sea level of the incoming and the reflected waves interfere constructively owing to the linear reflection. In addition, the combined effects of the western boundary reflection and the equatorial zonal winds in the western basin reduce the annual harmonic amplitude of the first baroclinic Kelvin wave in the western basin (see Fig. 11), which facilitates the dominance of semiannual oscillations in the total sea level there in spite of the strong local wind forcing at the annual period. If the decomposed Kelvin waves of the first four baroclinic modes should be replaced with the equatorially forced Kelvin waves in the reconstructed fields in Fig. 12, the sea level oscillations in the western basin would become annual dominant (not shown).

Except near the eastern boundary in winter, the Kelvin waves are found to contribute much less to the surface zonal currents than the Rossby waves. The semiannual oscillations of surface zonal currents over the equatorial Indian Ocean are primarily associated with the semiannual Rossby waves, the westward propagation of which gives rise to the progressive reversal of the equatorial Indian Ocean surface jets from the east to the west 4 times per year.

Acknowledgments. The authors thank NOAA/CDC, The Florida State University/COAPS, and the University of Texas/CSR for making the COADS data, FSU winds, and TOPEX/Poseidon data available on the Internet. We also thank Dr. A. J. Mariano for the ship drift data. Author W. Han is supported by NSF Grants OCE-0136836 and OCE-0452917. Author D. Yuan is supported by the "100 Experts" program of the Chinese Academy of Sciences.

REFERENCES

Boulanger, J. P., and C. Menkes, 1995: Propagation and reflection of long equatorial waves in the Pacific Ocean during the 1992–93 El Niño. *J. Geophys. Res.,* **100,** 25 041–25 059.

——, and L.-L. Fu, 1996: Evidence of boundary reflection of Kelvin and first-mode Rossby waves from TOPEX/Poseidon sea level data. *J. Geophys. Res.,* **101,** 16 361–16 371.

Cane, M., and E. S. Sarachik, 1977: Forced baroclinic ocean motions. II. The linear equatorial bounded case. *J. Mar. Res.,* **35,** 395–432.

——, and P. Gent, 1984: Reflection of low-frequency equatorial waves at arbitrary western boundaries. *J. Mar. Res.,* **42,** 487–502.

Gent, P., K. O'Neill, and M. Cane, 1983: A model of the semiannual oscillation in the equatorial Indian Ocean. *J. Phys. Oceanogr.,* **13,** 2148–2160.

Han, W., 2005: Origins and dynamics of the 90-day and 30–60-day variations in the equatorial Indian Ocean. *J. Phys. Oceanogr.,* **35,** 708–728.

——, J. P. McCreary, D. L. T. Anderson, and A. J. Mariano, 1999: Dynamics of the eastward surface jets in the equatorial Indian Ocean. *J. Phys. Oceanogr.,* **29,** 2191–2209.

——, P. J. Webster, R. Lukas, P. Hacker, and A. Hu, 2004: Impact of atmospheric intraseasonal variability in the Indian Ocean: Low-frequency rectification in equatorial surface current and transport. *J. Phys. Oceanogr.,* **34,** 1350–1372.

Hastenrath, S., and L. Greischar, 1991: The monsoonal current regimes of the tropical Indian Ocean: Observed surface flow fields and their geostrophic and wind-driven components. *J. Geophys. Res.,* **96,** 12 619–12 633.

Jensen, T. G., 1993: Equatorial variability and resonance in a wind-driven Indian Ocean model. *J. Geophys. Res.,* **98,** 22 533–22 552.

Jerlov, N. G., 1976: *Marine Optics*. Elsevier, 231 pp.

Knox, R., 1976: On a long series of measurements of Indian Ocean equatorial currents near Addu Atoll. *Deep-Sea Res.,* **23,** 211–221.

Large, W. G., J. C. McWilliams, and S. C. Doney, 1994: Oceanic vertical mixing: A review and a model with a nonlocal boundary layer parameterization. *Rev. Geophys.,* **32,** 363–403.

——, G. Danabasoglu, S. C. Doney, and J. C. McWilliams, 1997: Sensitivity to surface forcing and boundary layer mixing in a global ocean model: Annual-mean climatology. *J. Phys. Oceanogr.,* **27,** 2418–2447.

Le Blanc, J. L., and J. P. Boulanger, 2001: Propagation and reflection of long equatorial waves in the Indian Ocean from TOPEX/Poseidon data during the 1993–1998 period. *Climate Dyn.,* **17,** 547–557.

Levitus, S., and T. P. Boyer, 1994: *Temperature.* Vol. 4, *World Ocean Atlas 1994,* NOAA Atlas NESDIS 4, 117 pp.

——, R. Burgett, and T. P. Boyer, 1994: *Salinity.* Vol. 3, *World Ocean Atlas 1994,* NOAA Atlas NESDIS 3, 99 pp.

Luther, M. E., and J. J. O'Brien, 1985: Modelling the variability of the Somali Current. *Coherent Structures in Geophysical Turbulence,* J. C. Nihoul, Ed., Elsevier, 405–436.

Luyten, J., and D. Roemmich, 1982: Equatorial currents at semiannual period in the Indian Ocean. *J. Phys. Oceanogr.,* **12,** 406–413.

McCreary, J. P., 1981: A linear stratified ocean model of the equatorial undercurrent. *Quart. J. Roy. Soc. London,* **298A,** 603–635.

——, P. K. Kundo, and R. L. Molinari, 1993: A numerical investigation of dynamics and thermodynamics and mixed-layer processes in the Indian Ocean. *Progress in Oceanography,* Vol. 31, Pergamon, 181–244.

McPhaden, M. J., 1982a: Variability in the central Indian Ocean. Part I: Ocean dynamics. *J. Mar. Res.,* **40,** 157–176.

——, 1982b: Variability in the central Indian Ocean. Part II: Oceanic heat and turbulent balance. *J. Mar. Res.,* **40,** 403–419.

Minobe, S., and K. Takeuchi, 1995: Annual period equatorial waves in the Pacific Ocean. *J. Geophys. Res.,* **100,** 18 379–18 392.

O'Brien, J. J., and H. E. Hurlburt, 1974: An equatorial jet in the Indian Ocean, theory. *Science,* **184,** 1075–1077.

Reppin, J., F. A. Schott, and J. Fischer, 1999: Equatorial currents and transports in the upper central Indian Ocean: Annual cycle and interannual variability. *J. Geophys. Res.,* **104,** 15 495–15 514.

Reverdin, G., 1987: The upper equatorial Indian Ocean: The climatological seasonal cycle. *J. Phys. Oceanogr.,* **17,** 903–927.

Spall, M., and J. Pedlosky, 2005: Reflection and transmission of equatorial Rossby waves. *J. Phys. Oceanogr.,* **35,** 363–373.

Woodbury, K. E., M. E. Luther, and J. J. O'Brien, 1989: The wind-driven seasonal circulation in the southern tropical Indian Ocean. *J. Geophys. Res.,* **94,** 17 985–18 002.

Wyrtki, K., 1973: An equatorial jet in the Indian Ocean. *Science,* **181,** 262–264.

Yuan, D., 2005: The role of the Kelvin and Rossby waves in the seasonal cycle of the equatorial Pacific Ocean circulation. *J. Geophys. Res.,* **110,** C04004, doi:10.1029/2004JC002344.

——, M. M. Rienecker, and P. S. Schopf, 2004: Long wave dynamics of the interannual variability in a numerical hindcast of the equatorial Pacific Ocean circulation during the 1990s. *J. Geophys. Res.,* **109,** C05019, doi:10.1029/2003JC001936.

Zang, X., L.-L. Fu, and C. Wunsch, 2002: Observed reflectivity of the western boundary of the equatorial Pacific Ocean. *J. Geophys. Res.,* **107,** 3150, doi:10.1029/2000JC000719.